

Magic ELF: Image Deraining Meets Association Learning and Transformer

Kui Jiang
NERCMS, Wuhan University, China

Zhongyuan Wang*
NERCMS, Wuhan University, China

Chen Chen
CRCV, University of Central Florida
U.S.

Zheng Wang*
NERCMS, Wuhan University, China

Laizhong Cui
Shenzhen University, China

Chia-Wen Lin
National Tsing Hua University, China

ABSTRACT

Convolutional neural network (CNN) and Transformer have achieved great success in multimedia applications. However, little effort has been made to effectively and efficiently harmonize these two architectures to satisfy image deraining. This paper aims to unify these two architectures to take advantage of their learning merits for image deraining. In particular, the local connectivity and translation equivariance of CNN and the global aggregation ability of self-attention (SA) in Transformer are fully exploited for specific local context and global structure representations. Based on the observation that rain distribution reveals the degradation location and degree, we introduce degradation prior to help background recovery and accordingly present the association refinement deraining scheme. A novel multi-input attention module (MAM) is proposed to associate rain perturbation removal and background recovery. Moreover, we equip our model with effective depth-wise separable convolutions to learn the specific feature representations and trade off computational complexity. Extensive experiments show that our proposed method (dubbed as ELF) outperforms the state-of-the-art approach (MPRNet) by 0.25 dB on average, but only accounts for 11.7% and 42.1% of its computational cost and parameters. The source code is available at <https://github.com/kuijiang94/Magic-ELF>.

CCS CONCEPTS

• **Computing methodologies** → **Computer vision**; *Machine learning algorithms*.

KEYWORDS

Image Deraining, Self-attention, Association Learning

ACM Reference Format:

Kui Jiang, Zhongyuan Wang, Chen Chen, Zheng Wang, Laizhong Cui, and Chia-Wen Lin. 2022. Magic ELF: Image Deraining Meets Association Learning and Transformer. In *Proceedings of the 30th ACM International*

*Corresponding author

Permission to make digital or hard copies of all or part of this work for personal or classroom use is granted without fee provided that copies are not made or distributed for profit or commercial advantage and that copies bear this notice and the full citation on the first page. Copyrights for components of this work owned by others than ACM must be honored. Abstracting with credit is permitted. To copy otherwise, or republish, to post on servers or to redistribute to lists, requires prior specific permission and/or a fee. Request permissions from permissions@acm.org.

MM'22, October, 10–14, 2022, Lisbon, Portugal

© 2022 Association for Computing Machinery.

ACM ISBN xxxxxx...\$15.00

<https://doi.org/10.1185/xxxxxx>

Conference on Multimedia (MM'22) October, 10–14, 2022, Lisbon, Portugal.
ACM, New York, NY, USA, 10 pages. <https://doi.org/10.1185/xxxxxx>

1 INTRODUCTION

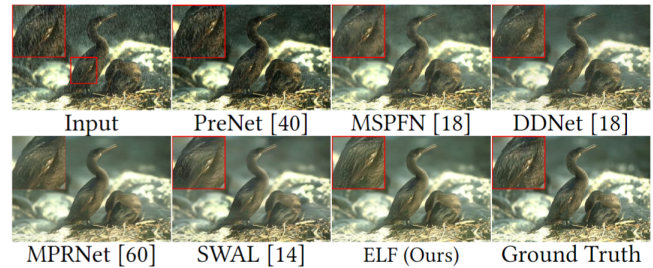


Figure 1: Visual comparison results. PreNet [40] and DRD-Net [18] remove rain streaks in some cases, but fail to cope with additional degradation effects of missing details and contrast bias. MPRNet [60] and SWAL [14] tend to smooth the contents while our ELF reconstructs credible textures. Please refer to the region highlighted in the red boxes for a close up comparison.

Rain perturbation causes detrimental effects on image quality and significantly degrades the performance of multimedia applications like image understanding [33, 47], object detection [67] and identification [52]. Image deraining [5, 20, 44] tends to produce the rain-free result from the rainy input, and has drawn widespread attention in the last decade. Prior to deep neural networks, the early model-based deraining methods [12] rely more on statistical analyses of image contents, and enforce handcrafted priors (e.g., sparsity and non-local means filtering) on both rain and background. Still, they are not robust to varying and complex rain conditions [2, 6, 66].

Because of the powerful ability to learn generalizable priors from large-scale data, CNNs have emerged as a preferable choice compared to conventional model-based methods. To further promote the deraining performance, various sophisticated architectures and training practices are designed to boost the efficiency and generalization [17, 55, 55, 57]. However, due to intrinsic characteristics of local connectivity and translation equivariance, CNNs have at least two shortcomings: 1) limited receptive field; 2) static weight of sliding window at inference, unable to cope with the content diversity. The former thus prevents the network from capturing the long-range pixel dependencies while the latter sacrifices the adaptability to the input contents. As a result, it is far from meeting the

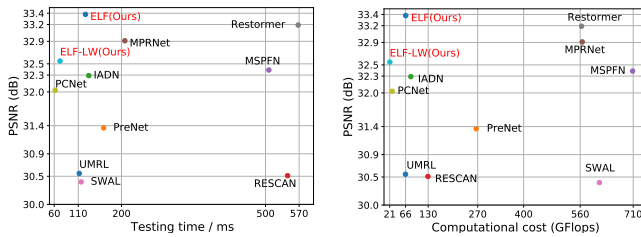


Figure 2: Comparison of mainstream deraining methods in terms of efficiency (inference time (ms) and computational cost (Gflops)) vs. performance (PSNR) on the TEST1200 dataset with image size of 512×512 . Compared with the top-performing method Restormer [18], our ELF achieves comparable deraining performance (33.38dB vs. 33.19dB) while saving 88.0% inference time (ms) (125 vs. 568) and 88.4% computational cost (Gflops) (66.39 vs. 568). Our light-weight model ELF-LW is still competitive, surpassing the real-time deraining method PCNet by 0.52dB while with less computation cost (Gflops) (21.53 vs. 28.21).

requirement in modeling the global rain distribution, and generates results with obvious rain residue (PreNet [40] and DRDNet [18]) or detail loss (MPRNet [60] and SWAL [14]). Please refer to the deraining results in Figure 1.

Self-attention (SA) calculates response at a given pixel by a weighted sum of all other positions, and thus has been explored in deep networks for various natural language and computer vision tasks [43, 49, 61]. Benefiting from the advantage of global processing, SA achieves significant performance boost over CNNs in eliminating the degradation perturbation [4, 32, 51]. However, due to the global calculation of SA, its computation complexity grows quadratically with the spatial resolution, making it infeasible to apply to high-resolution images [59]. More recently, Restormer [59] proposes a multi-Dconv head “transposed” attention (MDTA) block to model global connectivity, and achieves impressive deraining performance. Although MDTA applies SA across feature dimension rather than the spatial dimension and has linear complexity, still, Restormer quickly overtaxes the computing resources. As illustrated in Figure 2, the high-accuracy model Restormer [59] requires much more computation resource for a better restoration performance. It has 563.96 GFlops and 26.10 Million parameters, and consumes 0.568s to derain an image with 512×512 pixels using one TITAN X GPU, which is computationally or memory expensive for many real-world applications with resource-constrained devices.

Besides low efficiency, there are at least another two shortcomings for Restormer [59]. 1) Regarding the image deraining as a simple rain streaks removal problem based on the additive model is debatable, since the rain streak layer and background layer are highly interwoven, where rain streaks destroy image contents, including the details, color, and contrast. 2) Constructing a pure Transformer-based framework is suboptimal, since SA is good at aggregating global feature maps but immature in learning local contexture relations which CNNs are skilled at. That in turn naturally raises two questions: (1) How to associate the rain perturbation removal and background recovery? (2) How to unify SA and CNNs efficiently for image deraining?

To answer the first question, we take inspiration from the observation that rain distribution reflects the degradation location and degree, in addition to the rain distribution prediction. Therefore, we propose to refine background textures with the predicted degradation prior in an association learning manner. As a result, we accomplish the image deraining by associating rain streak removal and background recovery, where an image deraining network (IDN) and a background recovery network (BRN) are specifically designed for these two subtasks. The key part of association learning is a novel multi-input attention module (MAM). It generates the degradation prior and produces the degradation mask according to the predicted rainy distribution. Benefited from the global correlation calculation of SA, MAM can extract the informative complementary components from the rainy input (query) with the degradation mask (key), and then help accurate texture restoration.

An intuitive idea to deal with the second issue is to construct a unified model with the advantages of these two architectures. It has been demonstrated that the SA and standard convolution exhibit opposite behaviors but complementary [38]. Specifically, SA tends to aggregate feature maps with self-attention importance, but convolution diversifies them to focus on the local textures. Unlike Restormer equipped with pure Transformer blocks, we promote the design paradigm in a parallel manner of SA and CNNs, and propose a hybrid fusion network. It involves one residual Transformer branch (RTB) and one encoder-decoder branch (EDB) (The detailed pipeline is provided in [Supplementary](#)). The former takes a few learnable tokens (feature channels) as input and stacks multi-head attention and feed-forward networks to encode global features of the image. The latter, conversely, leverages the multi-scale encoder-decoder to represent contexture knowledge. We propose a light-weight hybrid fusion block (HFB) to aggregate the outcomes of RTB and EDB to yield a final solution to the subtask. In this way, we construct our final model as a two-stage Transformer-based method, namely ELF, for single image deraining, which **outperforms the CNN-based SOTA (MPRNet [60]) by 0.25dB on average, but saves 88.3% and 57.9% computational cost and parameters.**

The main contributions of this paper are summarized as follows.

- To the best of our knowledge, we are the first to consider the high efficiency and compatibility of Transformer and CNNs for the image deraining task, and unify the advantages of SA and CNNs into an association learning-based network for rain perturbation removal and background recovery. This showcases an efficient and effective implementation of part-whole hierarchy.
- We design a novel multi-input attention module (MAM) to associate rain streaks removal and background recovery tasks elaborately. It significantly alleviates the learning burden while promoting the texture restoration.
- Comprehensive experiments on image deraining and detection tasks have verified the effectiveness and efficiency of our proposed ELF method. ELF surpasses MPRNet [60] by 0.25dB on average, while the latter suffers from 8.5× computational cost and 2.4× parameters.

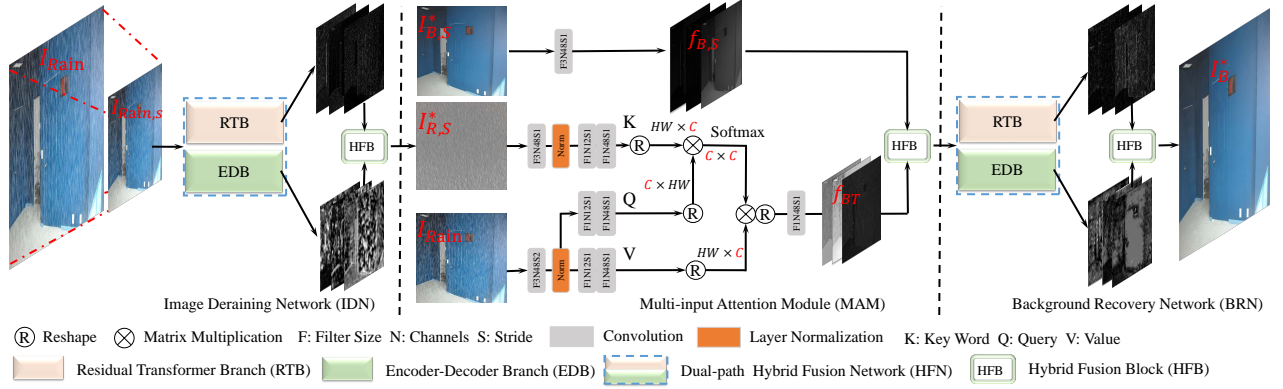


Figure 3: The architecture of our proposed ELF deraining method. It consists of an image deraining network (IDN), a multi-input attention module (MAM), and a background reconstruction network (BRN). IDN learns the corresponding rain distribution $I_{R,S}^*$ from the sub-sample $I_{Rain,S}$, and produces the corresponding deraining result $I_{B,S}^*$ by subtracting $I_{R,S}^*$. Then, MAM takes $I_{R,S}^*$, I_{Rain} and $I_{B,S}^*$ as inputs, where the predicted rain distribution provides the prior (local and degree) to exploit complementary background components f_{BT} from I_{Rain} to promote the background recovery.

2 RELATED WORK

Image deraining has achieved significant progress in innovative architectures and training methods in the last few years. Next, we briefly describe the typical models for image deraining and visual Transformer relative to our studies.

2.1 Single Image Deraining

Traditional deraining methods [23, 23, 36] adopt image processing techniques and hand-crafted priors to address the rain removal problem. However, these methods produce unsatisfied results when the predefined model do not hold. Recently, deep-learning based approaches [19, 27, 62] have emerged for rain streak removal and demonstrated impressive restoration performance. Early deep learning-based deraining approaches [9, 10] apply convolution neural networks (CNNs) to directly reduce the mapping range from input to output and produce rain-free results. To better represent the rain distribution, researchers take rain characteristics such as rain density [63], size and the veiling effect [27, 29] into account, and use recurrent neural networks to remove rain streaks via multiple stages [31] or the non-local network [45] to exploit long-range spatial dependencies for better rain streak removal [26]. Further, self-attention (SA) is recently introduced to eliminate the rain degradation with its powerful global correlation learning, and achieves impressive performance. Although the token compressed representation and global non-overlapping window-based SA [16, 51] are adopted to promote the global SA to alleviate the computational burden, these models still quickly overtaxes the computing resource. Apart from the low efficiency, these methods [16, 59] regard the deraining task as the rain perturbation removal only, ignoring the additional degradation effects of missing details and contrast bias.

2.2 Vision Transformers

Transformer-based models are first developed for sequence processing in natural language tasks [43]. Due to the distinguishing feature of the strong capability to learn long-range dependencies, ViT [8] introduces Transformer into computer vision field, and

then a plenty of Transformer-based methods have been applied to vision tasks such as image recognition [8, 15], segmentation [48], object detection [3, 35]. Vision Transformers [8, 42] decompose an image into a sequence of patches (local windows) and learn their mutual relationships, which is adaptable to the given input content [24]. Especially for low-level vision tasks, since the global feature representation promotes accurate texture inference, Transformer models have been employed to solve the low-level vision problems [32, 51]. For example, TTSR [53] proposes a self-attention module to transfer the texture information in the reference image to the high-resolution image reconstruction, which can deliver accurate texture features. Chen *et al.* [4] propose a pre-trained image processing transformer on the ImageNet datasets and uses the multi-head architecture to process different tasks separately. However, the direct application of SA fails to exploit the full potential of Transformer, resulting from heavy self-attention computation load and inefficient communications across different depth (scales) of layers. Moreover, little effort has been made to consider the intrinsic complementary characteristics between Transformer and CNNs to construct a compact and practical model. Naturally, this design choice restricts the context aggregation within local neighborhoods, defying the primary motivation of using self-attention over convolutions, thus not ideally suited for image-restoration tasks. In contrast, we propose to explore the bridge, and construct a hybrid model of Transformer and CNN for image deraining task.

3 PROPOSED METHOD

Our main goal is to construct a high-efficiency and high-accuracy deraining model by taking advantage of the CNN and Transformer. Theoretically, the self-attention (SA) averages feature map values with the positive importance-weights to learn the global representation while CNNs tend to aggregate the local correlated information. Intuitively, it is reasonable to combine them to fully exploit the local and global textures. A few studies try to combine these two structures to form a hybrid framework for low-level image restoration but have failed to give full play to it. Taking the image deraining as

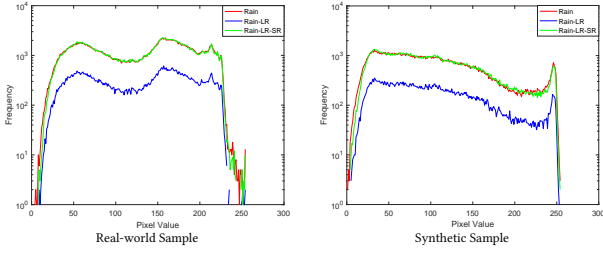


Figure 4: Fitting results of “Y” channel histogram for Real and Synthetic samples. “Rain” and “Rain-LR” denote the original and corresponding low-dimension space distribution of rainy image. “Rain-LR-SR” is the distribution via Bilinear interpolation from “Rain-LR”. The fitting results show that the reconstructed sampling space (“Rain-LR-SR”) from “Rain-LR” can get the similar statistical distribution with that of the original space.

an example, unlike the existing Transformer-based methods that directly apply Transformer blocks to replace convolutions, we consider the high efficiency and compatibility of these two structures, and construct a hybrid framework, dubbed ELF to harmonize their advantages for image deraining. Compared to the existing deraining methods, our proposed ELF departs from them in at least two key aspects. *Differences in design concepts:* unlike the additive composite model that predicts the optimal approximation I_B^* of background image I_B from the rainy image I_{Rain} , or learns the rain residue I_R^* and subtracting it to generate I_B^* , ELF casts the image deraining task into the composition of rain streak removal and background recovery, and introduces the Transformer to associate these two parts with a newly designed multi-input attention module (MAM). *Differences in composition:* since the low-frequency signals and high-frequency signals are informative to SA and convolutions [38], a dual-path framework is naturally constructed for the specific feature representation and fusion. Specifically, the backbone of ELF contains a dual-path hybrid fusion network, involving one residual Transformer branch (RTB) and one encoder-decoder branch (EDB) to characterize global structure (low-frequency components) and local textures (high-frequency components), respectively.

Figure 3 outlines the framework of our proposed ELF, which contains an image deraining network (IDN), a multi-input attention module (MAM), and a background recovery network (BRN). For efficiency, IDN and BRN share the same dual-path hybrid fusion network, which are elaborated in Section 3.2.

3.1 Pipeline and Model Optimization

Given a rainy image $I_{Rain} \in \mathbb{R}^{H \times W \times 3}$ and its clean version $I_B \in \mathbb{B}^{H \times W \times 3}$, where H and W denote the spatial height and weight, we observe that the reconstructed rainy image $I_{Rain,SR} \in \mathbb{R}^{H \times W \times 3}$ via bilinear interpolation from the sampled rainy image $I_{Rain,S} \in \mathbb{R}$ has the similar statistical distribution to the original one, shown in Figure 4. This inspires us to predict the rain streak distribution at sampling space to alleviate the learning and computational burden.

In this way, we first sample I_{Rain} and I_B with Bilinear operation to generate the corresponding sub-samples ($I_{Rain,S} \in \mathbb{R}$ and $I_{B,S} \in$

\mathbb{B}). As illustrated before, our ELF contains two subnetworks (IDN and BRN) to complete the image deraining via association learning. Thus, $I_{Rain,S}$ is then input to IDN to generate the corresponding rain distribution $I_{R,S}^*$ and deraining result $I_{B,S}^*$, expressed as

$$I_{R,S}^* = \mathcal{G}_{IDN}(F_{BS}(I_{Rain})), \quad (1)$$

where $F_{BS}(\cdot)$ denotes the Bilinear downsampling to generate the sampled rainy image $I_{Rain,S}$. $\mathcal{G}_{IDN}(\cdot)$ refers to the rain estimation function of IDN.

Rain distribution reveals the degradation location and degree, which is naturally reasonable to be translated into the degradation prior to help accurate background recovery. Before passing $I_{B,S}^*$ into BRN for background reconstruction, a multi-input attention module (MAM), shown in Figure 3, is designed to fully exploit the complementary background information from the rainy image I_{Rain} via the Transformer layer, and merge them to the embedding representation of $I_{B,S}^*$. These procedures of MAM are expressed as

$$\begin{aligned} f_{BT} &= F_{SA}(I_{R,S}^*, I_{Rain}), \\ f_{MAM} &= F_{HFB}(f_{BT}, F_B(I_{B,S}^*)). \end{aligned} \quad (2)$$

In Equation (2), $F_{SA}(\cdot)$ denotes self-attention functions, involving the embedding function and dot-product interaction. $F_B(\cdot)$ is the embedding function to generate the initial representation of $I_{B,S}^*$. $F_{HFB}(\cdot)$ refers to the fusion function in HFB. Following that, BRN takes f_{MAM} as input for background reconstruction as

$$I_B^* = \mathcal{G}_{BRN}(f_{MAM}) + F_{UP}(I_{B,S}^*), \quad (3)$$

where $\mathcal{G}_{BRN}(\cdot)$ denotes the super-resolving function of BRN, and $F_{UP}(\cdot)$ is the Bilinear upsampling.

Unlike the individual training of rain streak removal and background recovery, we introduce the joint constraint to enhance the compatibility of the deraining model with background recovery, automatically learned from the training data. Then the image loss (Charbonnier penalty loss [13, 22, 25]) and structural similarity (SSIM) [50] loss are employed to supervise networks to achieve the image and structural fidelity restoration simultaneously. The loss functions are given by

$$\begin{aligned} \mathcal{L}_{IDN} &= \sqrt{(I_{B,S}^* - I_{B,S})^2 + \varepsilon^2} + \alpha \times SSIM(I_{B,S}^*, I_{B,S}), \\ \mathcal{L}_{BRN} &= \sqrt{(I_B^* - I_B)^2 + \varepsilon^2} + \alpha \times SSIM(I_B^*, I_B), \\ \mathcal{L} &= \mathcal{L}_{IDN} + \lambda \times \mathcal{L}_{BRN}, \end{aligned} \quad (4)$$

where α and λ are used to balance the loss components, and experimentally set as -0.15 and 1 , respectively. The penalty coefficient ε is set to 10^{-3} .

3.2 Hybrid Fusion Network

It is known that the self-attention mechanism is the core part of Transformer, which is good at learning long-range semantic dependencies and capturing global structure representation in the image. Conversely, CNNs are skilled at modeling the local relations due to the intrinsic local connectivity. To this end, we construct the backbone of IDN and BRN into a deep dual-path hybrid fusion network by unifying the advantages of Transformer and CNNs. As shown in Figure 3, the backbone involves a residual Transformer branch (RTB) and an encoder-decoder branch (EDB). RTB takes a few

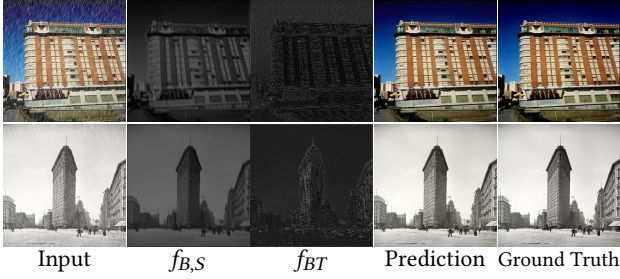


Figure 5: Visualization of MAM, including the embedding representation $f_{B,S}$ of background image and the extracted background texture information (f_{BT}). Using the complementary texture f_{BT} from the rainy image, the network can achieve more accurate background restoration. For a better visual effect, we respectively select three of the channels (48) from $f_{B,S}$ and f_{BT} , and then rescale their pixel values into $[0, 255]$ to generate the corresponding grayscale image.

learnable tokens (feature channels) as input and stacks multi-head attention and feed-forward networks to encode the global structure. However, capturing long-range pixel interactions is the culprit for the enormous amount of Transformer computational, making it infeasible to apply to high-resolution images, especially for the image restoration task. Besides processing the feature representation on the sampled space, inspired by [1], instead of learning the global spatial similarity, we apply SA to compute cross-covariance across channels to generate the attention map encoding the global context implicitly. It has linear complexity rather than quadratically complexity.

EDB is designed to infer locally-enriched textures. Inspired by U-Net [41], we also construct EDB with the U-shaped framework. The first three stages form the encoder, and the remaining three stages represent the decoder. Each stage takes a similar architecture, consisting of sampling layers, residual channel attention blocks (RCABs) [65] and hybrid fusion block. Instead of using the strided or transposed convolution for rescaling spatial resolution of features, we use Bilinear sampling followed by a 1×1 convolution layer to reduce checkerboard artifacts and model parameters. To facilitate residual feature fusion at different stages or scales, we design HFB to aggregate multiple inputs among stages in terms of the spatial and channel dimensions. HFB enables more diverse features to be fully used during the restoration process.

Moreover, to further reduce the number of parameters, RTB and EDB are equipped with depth-wise separable convolutions (DSC). For RTB, we integrate DSC into multi-head attention to emphasize on the local context before computing feature covariance to produce the global attention map. Moreover, we construct EDB into an asymmetric U-shaped structure, in which the encoder has the portable design with DSC, but the standard convolutions for the decoder. This scheme can save about 8% parameters of the whole network. We have experimentally verified that utilizing DSC in the encoder is better than that in the decoder.

3.3 Multi-input Attention Module

To associate rain streaks removal and background recovery, as shown in Figure 3, we construct a multi-input attention module

Table 1: Ablation study on the depth-wise separable convolutions (DSC), multi-input attention module (MAM), hybrid fusion block (HFB), SSIM loss, super-resolution (SR), residual Transformer branch (RTB) and encoder-decoder branch (EDB) on *Test1200* dataset. We obtain the model parameters (Million (M)), average inference time (Second (S)), and calculation complexity (GFlops (G)) of deraining on images with the size of 512×512 .

Model	SA	SR	DSC	HFB	MAM	SSIM	PSNR	SSIM	Par.	Time	GFlops
Rain Image	-	-	-	-	-	-	22.16	0.732	-	-	-
w/o SA	×	✓	✓	✓	✓	✓	32.78	0.919	1.536	50.24	50.24
w/o DSC	✓	✓	×	✓	✓	✓	32.73	0.918	1.518	0.121	62.37
w/o HFB	✓	✓	✓	×	✓	✓	32.56	0.917	1.539	0.102	69.41
w/o MAM	✓	✓	✓	✓	×	✓	31.46	0.906	1.516	0.121	64.28
w/o SSIM	✓	✓	✓	✓	✓	×	33.17	0.919	1.532	0.125	66.39
w/o all	×	✓	×	×	×	×	29.05	0.861	1.538	0.046	61.24
ELF*	✓	×	✓	✓	×	✓	32.97	0.921	1.519	0.156	214.67
ELF	✓	✓	✓	✓	✓	✓	33.38	0.925	1.532	0.125	66.39
Model	RTB		EDB		PSNR	SSIM	Par.	Time	GFlops		
w/o RTB	×		✓		31.29	0.910	1.536	0.041	26.48		
w/o EDB	✓		×		33.04	0.922	1.534	0.154	134.27		
ELF	✓		✓		33.38	0.925	1.532	0.125	66.39		

(MAM) with Transformer to fully exploit the complementary background information for enhancement. Unlike the standard Transformer receiving a sequence of image patches as input, MAM takes the predicted rain distribution $I_{R,S}^*$, sub-space deraining image ($I_{B,S}^*$) and rainy image I_{Rain} as inputs, and first learns the embedding representation ($f_{B,S}^*$, $f_{R,S}^*$, f_{Rain}), enriched with local contexts. $f_{R,S}^*$ and f_{Rain} serve as *query* (Q), *key* (K) and *value* (V) projections. Instead of learning the spatial attention map of size $\mathbb{R}^{HW \times HW}$, we then reshape query and key projections, and generate cross-covariance transposed-attention map $M \in \mathbb{R}^{C \times C}$ via the dot-product interaction between $f_{R,S}^*$ and f_{Rain} . As shown in Figure 5, the attention map guides the network to excavate background texture information (f_{BT}) from the embedding representation (f_{Rain}) of I_{Rain} . The procedures in SA are expressed as

$$F_{SA} = (\text{Softmax}(F_K(I_{R,S}^*) \circ F_Q(I_{Rain})) \circ F_V(I_{Rain})), \quad (5)$$

where $F_K(\cdot)$, $F_Q(\cdot)$ and $F_V(\cdot)$ are the embedding functions to produce the projections. \circ and $F_S(\cdot)$ denote the dot-product interaction and softmax function. Followed by a hybrid fusion block, the extracted complementary information is merged with the embedding presentation of $I_{B,S}^*$ to enrich background representation.

3.4 Hybrid Fusion Block

Considering the feature redundancy and knowledge discrepancy among residual blocks and encoding stages, we introduce a novel hybrid fusion block (HFB) where the low-level contextualized features of earlier stages help consolidate high-level features of the later stages (or scales). Specifically, we incorporate depth-wise separable convolutions and the channel attention layer into HFB to discriminatively aggregate multi-scale features in spatial and channel dimensions. Compared to skip pixel-wise superimposition or convolution fusion, our HFB is more flexible and effective.

4 EXPERIMENTS

To validate our proposed ELF, we conduct extensive experiments on synthetic and real-world rainy datasets, and compare ELF with several mainstream image deraining methods. These methods include MPRNet [60], SWAL [14], RCDNet [46], DRDNet [7], MSPFN [18], IADN [17], PreNet [40], UMRL [56], DIDMDN [63], RESCAN [31] and DDC [30]. Five commonly used evaluation metrics, such as Peak Signal to Noise Ratio (PSNR), Structural Similarity (SSIM), Feature Similarity (FSIM), Naturalness Image Quality Evaluator (NIQE) [37] and Spatial-Spectral Entropy-based Quality (SSEQ) [34], are employed for comparison.

4.1 Implementation Details

Data Collection. Since there exists the discrepancy in training samples for all comparison methods, following [17, 18], we use 13,700 clean/rain image pairs from [10, 64] for training all comparison methods with their publicly released codes by tuning the optimal settings for a fair comparison. For testing, four synthetic benchmarks (Test100 [64], Test1200 [63], R100H and R100L [54]) and three real-world datasets (Rain in Driving (RID), Rain in Surveillance (RIS) [28] and Real127 [63]) are considered for evaluation.

Experimental Setup. In our baseline, the number of Transformer blocks in RTB is set to 10 while RCAB is empirically set to 1 for each stage in EDB with filter numbers of 48. The training images are coarsely cropped into small patches with a fixed size of 256×256 pixels to obtain the training samples. We use Adam optimizer with the learning rate (2×10^{-4}) with the decay rate of 0.8 at every 65 epochs till 600 epochs and batch size (12) to train our ELF on a single Titan Xp GPU.

4.2 Ablation Study

Validation on Basic Components. We conduct ablation studies to validate the contributions of individual components, including the self-attention (SA), depth-wise separable convolutions (DSC), super-resolution reconstruction (SR), hybrid fusion block (HFB) and multi-input attention module (MAM) to the final deraining performance. For simplicity, we denote our final model as ELF and devise the baseline model *w/o* all by removing all these components above. Quantitative results in terms of deraining performance and inference efficiency on the Test1200 dataset are presented in Table 1, revealing that the complete deraining model ELF achieves significant improvements over its incomplete versions. Compared to *w/o* MAM model (removing MAM from ELF), ELF achieves 1.92dB performance gain since the association learning in MAM can help the network to fully exploit the background information from the rainy input with the predicted rain distribution prior. In addition, disentangling the image deraining task into rain streaks removal and texture reconstruction at the low-dimension space exhibits considerable superiority in terms of efficiency (19.8% and 67.6% more efficient in inference time and computational cost, respectively) and restoration quality (referring to the results of ELF and ELF* models (accomplishing the deraining and texture recovery at the original resolution space [7])). Moreover, using the depth-wise separable convolution allows increasing the channel depth with approximately the same parameters, thus enhancing the representation capacity (referring to the results of ELF and *w/o* DSC models).

Compared to the *w/o* SA that replaces the Transformer blocks in RTB with the standard RCABs, ELF gains 0.45dB improvement with acceptable computational cost.

We also conduct ablation studies to validate the dual-path hybrid fusion framework, involving an residual Transformer branch (RTB) and a U-shaped encoder-decoder branch (EDB). Based on ELF, we devise two comparison models (*w/o* RTB and *w/o* EDB) by removing these two branches in turn. Quantitative results are presented in Table 1. Removing RTB may greatly weaken the representation capability on the spatial structure, leading to the obvious performance decline (2.09dB in PSNR) (referring to the results of ELF and *w/o* RTB models). Moreover, EDB allows the network to aggregate multi-scale textural features, which is crucial to enrich the representation of local textures.

4.3 Comparison with State-of-the-arts

Synthesized Data. Quantitative results on Test1200, Test100, 100H and R100L datasets are provided in Table 2. Meanwhile, the inference time, model parameters and computational cost are also compared. It is observed that most of the deraining models obtain impressive performance on light rain cases with high consistency. However, only our ELF and MPRNet still perform favorably on heavy rain conditions, exhibiting great superiority over other competing methods in terms of PSNR. As expected, our ELF model achieves the best scores on all metrics, **surpassing the CNN-based SOTA (MPRNet) by 0.25 dB on average, but only accounts for its 11.7% and 42.1% computational cost and parameters.** Meanwhile, our light-weight deraining model ELF-LW is still competitive, which gains the third-best average PSNR score on four datasets. In particular, ELF-LW averagely surpasses the real-time image deraining method PCNet [21] by 1.08dB, while with less parameters (saving 13.6%) and computational cost (saving 23.7%).

For more convincing evidence, we also provide visual comparisons in Figure 6. High-accuracy methods, such as PreNet, MSPFN and RCDNet, can effectively eliminate the rain layer and thus bring an improvement in visibility. But they fail to generate visual appealing results *by introducing considerable artifacts and unnatural color appearance*, the heavy rain condition in particular. Likewise, DRDNet focuses on the detail recovery, but shows undesired deraining performance. MPRNet tends to produce over-smoothing results. Besides recovering cleaner and more credible image textures, our ELF produces results with better contrast and less color distortion. Please refer to the “tiger” and “horse” scenarios. Moreover, we provide the comparison and analyses in terms of the color histogram fitting curve of “Y” channel in [Supplementary](#), which verifies the consistency between the predicted deraining result to the ground truth in terms of the statistic distribution. We speculate that these visible improvements on restoration quality may benefit from our proposed hybrid representation framework of Transformer and CNN as well as the association learning scheme for rain streak removal and background recovery. These strategies are integrated into a unified framework, allowing the network to fully exploit the respective learning merits for image deraining while guaranteeing the inference efficiency.

Real-world Data. We further conduct experiments on three real-world datasets: Real127 [63], Rain in Driving (RID), and Rain in

Table 2: Comparison results of average PSNR, SSIM, and FSIM on Test100/Test1200/R100H/R100L datasets. When averaged across all four datasets, our ELF advances state-of-the-art (MPRNet) by 0.25 dB, but accounts for only its 11.7% and 42.1% computational cost and parameters. We obtain the model parameters (Million) and average inference time (Second) of deraining on images with the size of 512× 512. * denotes the recursive network using the parameter sharing strategy. ELF-LW denotes the light-weight version of our ELF with the number of Transformer blocks to 5 and channels to 32.

Methods	RESCAN* [31]	UMRL [56]	PreNet* [40]	IADN [17]	MSPFN [18]	DRDNet [7]	PCNet [21]	MPRNet [60]	SWAL [14]	ELF-LW (Ours)	ELF (Ours)
Test100/Test1200											
Datasets											
PSNR	25.00/30.51	24.41/30.55	24.81/31.36	26.71/32.29	27.50/32.39	28.06/26.73	26.17/32.03	30.27/32.91	28.47/30.40	29.41/32.55	30.45/33.38
SSIM	0.835/0.882	0.829/0.910	0.851/0.911	0.865/0.916	0.876/0.916	0.874/0.824	0.871/0.913	0.897/0.916	0.889/0.892	0.894/0.912	0.909/0.925
FSIM	0.909/0.944	0.910/0.955	0.916/0.955	0.924/0.958	0.928/0.960	0.925/0.920	0.924/0.956	0.939/0.960	0.936/0.950	0.937/0.960	0.945/0.964
R100H/R100L											
Datasets											
PSNR	26.36/29.80	26.01/29.18	26.77/32.44	27.86/32.53	28.66/32.40	21.21/29.24	28.45/34.42	30.41/36.40	29.30/34.60	28.83/34.61	30.48/36.67
SSIM	0.786/0.881	0.832/0.923	0.858/0.950	0.835/0.934	0.860/0.933	0.668/0.883	0.871/0.952	0.889/0.965	0.887/0.958	0.876/0.958	0.896/0.968
FSIM	0.864/0.919	0.876/0.940	0.890/0.956	0.875/0.942	0.890/0.943	0.797/0.903	0.897/0.959	0.910/0.969	0.908/0.963	0.901/0.962	0.915/0.972
Avg-PSNR↑	27.91	27.53	28.84	29.84	30.23	26.31	30.27	32.49	30.69	31.35	32.74
Par.(M)↓	0.150	0.984	0.169	0.980	13.35	5.230	0.655	3.637	156.54	0.566	1.532
Time (S)↓	0.546	0.112	0.163	0.132	0.507	1.426	0.062	0.207	0.116	0.072	0.125
GFlops (G)↓	129.28	65.74	265.76	80.99	708.39	–	28.21	565.81	614.35	21.53	66.39

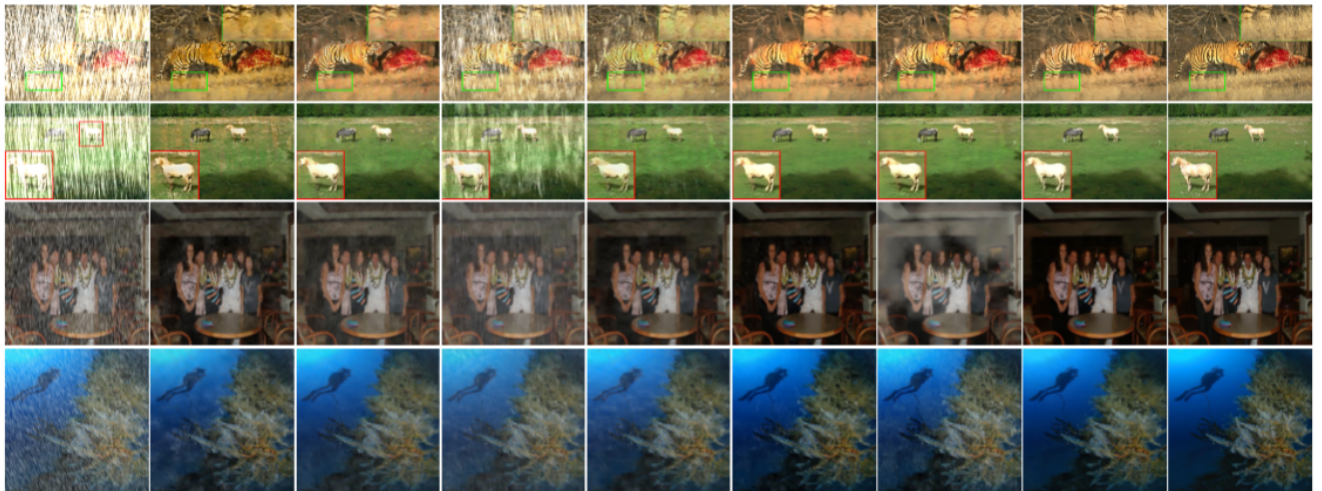


Figure 6: Visual comparison of derained images obtained by seven methods on R100H/R100L (1st – 2th rows) and Test100/Test1200 (3rd – 4th rows) datasets. Please refer to the region highlighted in the boxes for a close up comparison.

Table 3: Comparison of average NIQE/SSEQ scores with ten deraining methods on three real-world datasets.

Datasets	DIDMDN	RESCAN [31]	DDC [30]	LPNet [11]	UMRL [56]	PreNet [40]	IADN [17]	MSPFN [18]	DRDNet [7]	MPRNet [60]	ELF (Ours)
Real127 (127)	3.929/32.42	3.852/30.09	4.022/29.33	3.989/29.62	3.984/29.48	3.835/29.61	3.769/29.12	3.816/29.05	4.208/30.34	3.965/30.05	3.735/29.16
RID (2495)	5.693/41.71	6.641/40.62	6.247/40.25	6.783/42.06	6.757/41.04	7.007/43.04	6.035/40.72	6.518/40.47	5.715/39.98	6.452/40.16	4.318/37.89
RIS (2348)	5.751/46.63	6.485/50.89	5.826/47.80	6.396/53.09	5.615/43.45	6.722/48.22	5.909/42.95	6.135/43.47	6.269/45.34	6.610/48.78	5.835/42.16

Surveillance (RIS) [28]. Quantitative results of NIQE [37] and SSEQ [34] are listed in Table 3, where smaller NIQE and SSEQ scores indicate better perceptual quality and clearer contents. Again, our proposed ELF is highly competitive, achieving the lowest average values on the RID dataset and the best best average scores of NIQE and SSEQ on the Real127 and RIS datasets, respectively. We visualize the deraining results in Figure 7, showing that ELF produces rain-free images with cleaner and more credible contents, whereas the competing methods fail to remove rain streaks. These evidences indicate

that our ELF model performs well in eliminating rain perturbation while preserving textural details and image naturalness.

4.4 Impact on Downstream Vision Tasks

Eliminating the degraded effects of rain streaks under rainy conditions while preserving credible textural details is crucial for object detection. This motivates us to investigate the effect of deraining performance on object detection accuracy based on popular object detection algorithms (e.g., YOLOv3 [39]). Based on our ELF and

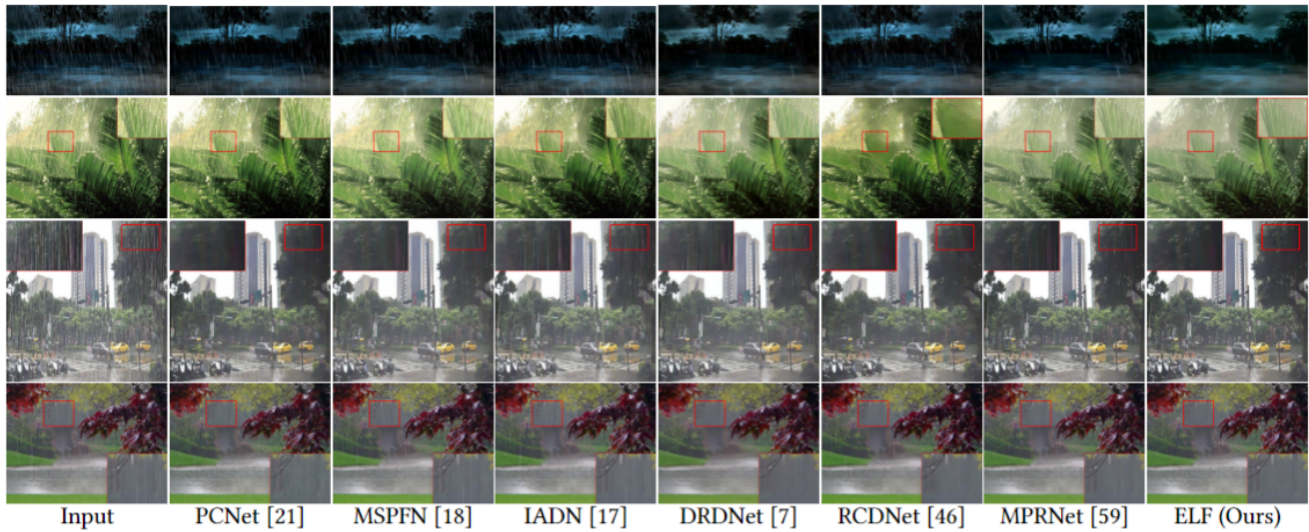


Figure 7: Visual comparison of derained images obtained by eight methods on five **real-world scenarios**, covering rain veiling effect (1st), heavy rain (2st) and light rain (3st-4st). Please refer to the region highlighted in the boxes for a close up comparison.

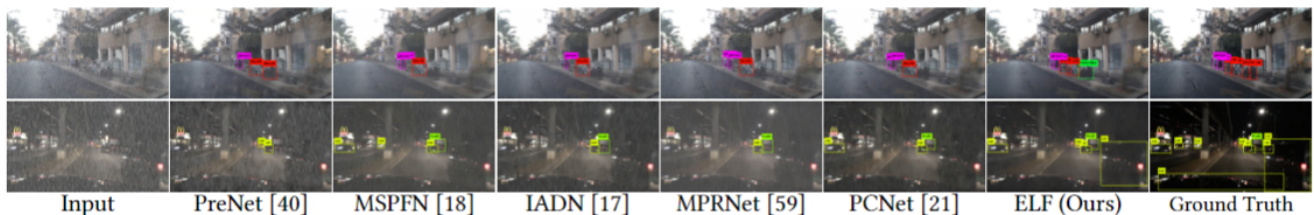


Figure 8: Visual comparison of joint image deraining and object detection on BDD350 dataset.

Table 4: Comparison results of joint image deraining and object detection on COCO350/BDD350 datasets.

Methods	Rain input	RESCAN [31]	PreNet [40]	IADN [17]	MSPFN [18]	MPRNet [60]	ELF-LW	ELF (Ours)
Deraining; Dataset: COCO350/BDD350; Image Size: 640× 480/1280× 720								
PSNR	14.79/14.13	17.04/16.71	17.53/16.90	18.18/17.91	18.23/17.85	17.99/16.83	18.43/18.09	18.93/18.49
SSIM	0.648/0.470	0.745/0.646	0.765/0.652	0.790/0.719	0.782/ 0.761	0.769/0.622	0.800/0.714	0.818/0.761
Ave.inf.time (s)	-/-	0.546/1.532	0.227/0.764	0.135/0.412	0.584/1.246	0.181/0.296	0.076/0.160	0.128/0.263
Object Detection; Algorithm: YOLOv3; Dataset: COCO350/BDD350; Threshold: 0.6								
Precision (%)	23.03/36.86	28.74/40.33	31.31/38.66	32.92/40.28	32.56/41.04	31.31/40.49	33.31/40.88	33.85/41.84
Recall (%)	29.60/42.80	35.61/47.79	37.92/48.59	39.83/50.25	39.31/50.40	38.98/48.77	40.43/51.55	40.43/52.60
IoU (%)	55.50/59.85	59.81/61.98	60.75/61.08	61.96/62.27	61.69/62.42	61.14/61.99	62.21/62.48	62.61/62.80

several representative deraining methods, the restoration procedures are directly applied to the rainy images to generate corresponding rain-free outputs. We then apply the publicly available pre-trained models of YOLOv3 for the detection task. Table 4 shows that ELF achieves highest PSNR scores on COCO350 and BDD350 datasets [18]. Meanwhile, the rain-free results generated by ELF facilitate better object detection performance than other deraining methods. Visual comparisons on two instances in Figure 8 indicate that the deraining images by ELF exhibit a notable superiority in

terms of image quality and detection accuracy. We attribute the considerable performance improvements of both deraining and down-stream detection tasks to our association learning between rain streaks removal and detail recovery tasks.

4.5 Robust Analyses on Adversarial Attacks

We conduct a brief study on the robustness of mainstream rain removal methods against adversarial attacks, including the LMSE

attack and LPIPS attacks [58]. Our study shows that the deraining models are more vulnerable to the adversarial attacks perturbations while our method shows better robustness over other competitors. More details and analyses are included in [Supplementary](#).

5 CONCLUSION

We rethink the image deraining as a composite task of rain streak removal, textures recovery and their association learning, and propose a dynamic associated network (ELF) for image deraining. Accordingly, a two-stage architecture and an associated learning module (ALM) are adopted in ELF to account for twin goals of rain streak removal and texture reconstruction while facilitating the learning capability. Meanwhile, the joint optimization promotes the compatibility while maintaining the model compactness. Extensive results on image deraining and joint detection task demonstrate the superiority of our ELF model over the state-of-the-arts.

ACKNOWLEDGMENTS

This work is supported by National Natural Science Foundation of China (U1903214, 62071339, 62072347, 62171325), Natural Science Foundation of Hubei Province (2021CFB464) Guangdong-Macao Joint Innovation Project (2021A0505080008) Open Research Fund from Guangdong Laboratory of Artificial Intelligence and Digital Economy (SZ)(GML-KF-22-16).

REFERENCES

- [1] Alaaeldin Ali, Hugo Touvron, Mathilde Caron, Piotr Bojanowski, Matthijs Douze, Armand Joulin, Ivan Laptev, Natalia Neverova, Gabriel Synnaeve, Jakob Verbeek, et al. 2021. Xcit: Cross-covariance image transformers. *Advances in neural information processing systems* 34 (2021).
- [2] Jérémie Bossu, Nicolas Hautière, and Jean-Philippe Tarel. 2011. Rain or snow detection in image sequences through use of a histogram of orientation of streaks. *IJCV* 93, 3 (2011), 348–367.
- [3] Nicolas Carion, Francisco Massa, Gabriel Synnaeve, Nicolas Usunier, Alexander Kirillov, and Sergey Zagoruyko. 2020. End-to-end object detection with transformers. In *European conference on computer vision*. Springer, 213–229.
- [4] Hanting Chen, Yunhe Wang, Tianyu Guo, Chang Xu, Yiping Deng, Zhenhua Liu, Siwei Ma, Chunjing Xu, Chao Xu, and Wen Gao. 2021. Pre-trained image processing transformer. In *Proceedings of the IEEE/CVF Conference on Computer Vision and Pattern Recognition*. 12299–12310.
- [5] Xiang Chen, Jinshan Pan, Kui Jiang, Yufeng Li, Yufeng Huang, Caihua Kong, Longgang Dai, and Zhentao Fan. 2022. Unpaired Deep Image Deraining Using Dual Contrastive Learning. In *Proceedings of the IEEE/CVF Conference on Computer Vision and Pattern Recognition*. 2017–2026.
- [6] Yi-Lei Chen and Chiou-Ting Hsu. 2013. A generalized low-rank appearance model for spatio-temporally correlated rain streaks. In *CVPR*. 1968–1975.
- [7] S. Deng, M. Wei, J. Wang, Y. Feng, L. Liang, H. Xie, F. L. Wang, and M. Wang. 2020. Detail-recovery Image Deraining via Context Aggregation Networks. In *CVPR*. 14548–14557. <https://doi.org/10.1109/CVPR42600.2020.01457>
- [8] Alexey Dosovitskiy, Lucas Beyer, Alexander Kolesnikov, Dirk Weissenborn, Xiuhua Zhai, Thomas Unterthiner, Mostafa Dehghani, Matthias Minderer, Georg Heigold, Sylvain Gelly, et al. 2020. An image is worth 16x16 words: Transformers for image recognition at scale. *arXiv preprint arXiv:2010.11929* (2020).
- [9] Xueyang Fu, Jiabin Huang, Xinghao Ding, Yinghao Liao, and John Paisley. 2017. Clearing the skies: A deep network architecture for single-image rain removal. *IEEE Trans. Image Process.* 26, 6 (2017), 2944–2956.
- [10] Xueyang Fu, Jiabin Huang, Delu Zeng, Yue Huang, Xinghao Ding, and John Paisley. 2017. Removing rain from single images via a deep detail network. In *CVPR*. 3855–3863.
- [11] X. Fu, B. Liang, Y. Huang, X. Ding, and J. Paisley. 2020. Lightweight Pyramid Networks for Image Deraining. *IEEE TNNLS* 31, 6 (2020), 1794–1807.
- [12] Kshitiz Garg and Shree K Nayar. 2005. When does a camera see rain?. In *ICCV*, Vol. 2. 1067–1074.
- [13] Mengshun Hu, Kui Jiang, Liang Liao, Jing Xiao, Junjun Jiang, and Zheng Wang. 2022. Spatial-Temporal Space Hand-in-Hand: Spatial-Temporal Video Super-Resolution via Cycle-Projected Mutual Learning. In *Proceedings of the IEEE/CVF Conference on Computer Vision and Pattern Recognition*. 3574–3583.
- [14] Huaibo Huang, Aijing Yu, Zhenhua Chai, Ran He, and Tieniu Tan. 2021. Selective Wavelet Attention Learning for Single Image Deraining. *International Journal of Computer Vision* 129, 4 (2021), 1282–1300.
- [15] Momal Ijaz, Renato Diaz, and Chen Chen. 2022. Multimodal Transformer for Nursing Activity Recognition. In *Proceedings of the IEEE/CVF Conference on Computer Vision and Pattern Recognition*. 2065–2074.
- [16] Haobo Ji, Xin Feng, Wenjie Pei, Jinxing Li, and Guangming Lu. 2021. U2Former: A Nested U-shaped Transformer for Image Restoration. *arXiv preprint arXiv:2112.02279* (2021).
- [17] K. Jiang, Z. Wang, P. Yi, C. Chen, Z. Han, T. Lu, B. Huang, and J. Jiang. 2020. Decomposition Makes Better Rain Removal: An Improved Attention-guided Deraining Network. *IEEE Trans. Circuits Syst. Video Technol.* (2020), 1–1. <https://doi.org/10.1109/TCSVT.2020.3044887>
- [18] K. Jiang, Z. Wang, P. Yi, C. Chen, B. Huang, Y. Luo, J. Ma, and J. Jiang. 2020. Multi-Scale Progressive Fusion Network for Single Image Deraining. In *CVPR*. 8343–8352.
- [19] Kui Jiang, Zhongyuan Wang, Peng Yi, Chen Chen, Guangcheng Wang, Zhen Han, Junjun Jiang, and Zixiang Xiong. 2021. Multi-scale hybrid fusion network for single image deraining. *IEEE Transactions on Neural Networks and Learning Systems* (2021).
- [20] Kui Jiang, Zhongyuan Wang, Peng Yi, Chen Chen, Xiaofen Wang, Junjun Jiang, and Zixiang Xiong. 2021. Multi-level memory compensation network for rain removal via divide-and-conquer strategy. *IEEE Journal of Selected Topics in Signal Processing* 15, 2 (2021), 216–228.
- [21] Kui Jiang, Zhongyuan Wang, Peng Yi, Chen Chen, Zheng Wang, Xiao Wang, Junjun Jiang, and Chia-Wen Lin. 2021. Rain-free and residue hand-in-hand: A progressive coupled network for real-time image deraining. *IEEE Trans. Image Process.* 30 (2021), 7404–7418.
- [22] Kui Jiang, Zhongyuan Wang, Peng Yi, and Junjun Jiang. 2020. Hierarchical dense recursive network for image super-resolution. *Pattern Recognition* 107 (2020), 107475.
- [23] Li-Wei Kang, Chia-Wen Lin, and Yu-Hsiang Fu. 2012. Automatic single-frame-based rain streaks removal via image decomposition. *IEEE Trans. Image Process.* 21, 4 (2012), 3888–3901.
- [24] Salman Khan, Muzammal Naseer, Munawar Hayat, Syed Waqas Zamir, Fahad Shahbaz Khan, and Mubarak Shah. 2021. Transformers in vision: A survey. *ACM Computing Surveys (CSUR)* (2021).
- [25] Wei-Sheng Lai, Jia-Bin Huang, Narendra Ahuja, and Ming-Hsuan Yang. 2017. Deep laplacian pyramid networks for fast and accurate super-resolution. In *CVPR*. 624–632.
- [26] Guanbin Li, Xiang He, Wei Zhang, Huiyou Chang, Le Dong, and Liang Lin. 2018. Non-locally Enhanced Encoder-Decoder Network for Single Image De-raining. (2018), 1056–1064.
- [27] Ruoteng Li, Loong Fah Cheong, and Robby T Tan. 2017. Single Image Deraining using Scale-Aware Multi-Stage Recurrent Network. (2017).
- [28] Siyuan Li, Iago Breno Araujo, Wenqi Ren, Zhangyang Wang, Eric K Tokuda, Roberto Hirata Junior, Roberto Cesar-Junior, Jiawan Zhang, Xiaojie Guo, and Xiaochun Cao. 2019. Single image deraining: A comprehensive benchmark analysis. In *CVPR*. 3838–3847.
- [29] Siyuan Li, Wenqi Ren, Jiawan Zhang, Jinke Yu, and Xiaojie Guo. 2019. Single image rain removal via a deep decomposition-composition network. *CVIU* 186 (2019), 48–57.
- [30] Siyuan Li, Wenqi Ren, Jiawan Zhang, Jinke Yu, and Xiaojie Guo. 2019. Single image rain removal via a deep decomposition-composition network. *CVIU* 186 (2019), 48–57.
- [31] Xia Li, Jianlong Wu, Zhouchen Lin, Hong Liu, and Hongbin Zha. 2018. Recurrent squeeze-and-excitation context aggregation net for single image deraining. In *ECCV*. 254–269.
- [32] Jingyun Liang, Jiezhong Cao, Guolei Sun, Kai Zhang, Luc Van Gool, and Radu Timofte. 2021. Swinir: Image restoration using swin transformer. In *Proceedings of the IEEE/CVF International Conference on Computer Vision*. 1833–1844.
- [33] Liang Liao, Wenyi Chen, Jing Xiao, Zheng Wang, Chia-Wen Lin, and Shin'ichi Satoh. 2022. Unsupervised Foggy Scene Understanding via Self Spatial-Temporal Label Diffusion. *IEEE Transactions on Image Processing* 31 (2022), 3525–3540.
- [34] Lixiong Liu, Bao Liu, Hua Huang, and Alan Conrad Bovik. 2014. No-reference image quality assessment based on spatial and spectral entropies. *SPIC* 29, 8 (2014), 856–863.
- [35] Ze Liu, Yutong Lin, Yue Cao, Han Hu, Yixuan Wei, Zheng Zhang, Stephen Lin, and Baining Guo. 2021. Swin transformer: Hierarchical vision transformer using shifted windows. In *Proceedings of the IEEE/CVF International Conference on Computer Vision*. 10012–10022.
- [36] Y. Luo, Y. Xu, and H. Ji. 2015. Removing Rain from a Single Image via Discriminative Sparse Coding. In *ICCV*. 3397–3405.
- [37] Anish Mittal, Rajiv Soundararajan, and Alan C Bovik. 2012. Making a “completely blind” image quality analyzer. *IEEE Signal Process. Lett.* 20, 3 (2012), 209–212.
- [38] Namuk Park and Songkuk Kim. 2022. How Do Vision Transformers Work?. In *ICLR*.

- [39] Joseph Redmon and Ali Farhadi. 2018. Yolov3: An incremental improvement. *arXiv preprint arXiv:1804.02767* (2018).
- [40] Dongwei Ren, Wangmeng Zuo, Qinghua Hu, Pengfei Zhu, and Deyu Meng. 2019. Progressive image deraining networks: a better and simpler baseline. In *CVPR*. 3937–3946.
- [41] Olaf Ronneberger, Philipp Fischer, and Thomas Brox. 2015. U-net: Convolutional networks for biomedical image segmentation. In *MICCAI*. 234–241.
- [42] Hugo Touvron, Matthieu Cord, Matthijs Douze, Francisco Massa, Alexandre Sablayrolles, and Hervé Jégou. 2021. Training data-efficient image transformers & distillation through attention. In *International Conference on Machine Learning*. PMLR, 10347–10357.
- [43] Ashish Vaswani, Noam Shazeer, Niki Parmar, Jakob Uszkoreit, Llion Jones, Aidan N Gomez, Łukasz Kaiser, and Illia Polosukhin. 2017. Attention is all you need. *Advances in neural information processing systems* 30 (2017).
- [44] Cong Wang, Xiaoying Xing, Yutong Wu, Zhixun Su, and Junyang Chen. 2020. DCSFN: Deep Cross-scale Fusion Network for Single Image Rain Removal. In *ACM Multimedia*. 1643–1651.
- [45] H. Wang, Q. Xie, Q. Zhao, and D. Meng. 2020. A Model-Driven Deep Neural Network for Single Image Rain Removal. In *CVPR*. 3100–3109.
- [46] Hong Wang, Qi Xie, Qian Zhao, and Deyu Meng. 2020. A model-driven deep neural network for single image rain removal. In *Proceedings of the IEEE/CVF Conference on Computer Vision and Pattern Recognition*. 3103–3112.
- [47] Wenxuan Wang, Chen Chen, Jing Wang, Sen Zha, Yan Zhang, and Jiangyun Li. 2022. Med-DANet: Dynamic Architecture Network for Efficient Medical Volumetric Segmentation. *arXiv preprint arXiv:2206.06575* (2022).
- [48] Wenhai Wang, Enze Xie, Xiang Li, Deng-Ping Fan, Kaitao Song, Ding Liang, Tong Lu, Ping Luo, and Ling Shao. 2021. Pyramid vision transformer: A versatile backbone for dense prediction without convolutions. In *Proceedings of the IEEE/CVF International Conference on Computer Vision*. 568–578.
- [49] Xiaolong Wang, Ross Girshick, Abhinav Gupta, and Kaiming He. 2018. Non-local neural networks. In *CVPR*. 7794–7803.
- [50] Zhou Wang, Alan C Bovik, Hamid R Sheikh, Eero P Simoncelli, et al. 2004. Image quality assessment: from error visibility to structural similarity. *IEEE Trans. Image Process.* 13, 4 (2004), 600–612.
- [51] Zhendong Wang, Xiaodong Cun, Jianmin Bao, and Jianzhuang Liu. 2021. Uformer: A general u-shaped transformer for image restoration. *arXiv preprint arXiv:2106.03106* (2021).
- [52] Pengyu Xie, Xin Xu, Zheng Wang, and Toshihiko Yamasaki. 2022. Sampling and Re-weighting: Towards Diverse Frame Aware Unsupervised Video Person Re-identification. *IEEE Transactions on Multimedia* (2022).
- [53] Fuzhi Yang, Huan Yang, Jianlong Fu, Hongtao Lu, and Baining Guo. 2020. Learning texture transformer network for image super-resolution. In *Proceedings of the IEEE/CVF conference on computer vision and pattern recognition*. 5791–5800.
- [54] Wenhao Yang, Robby T Tan, Jiashi Feng, Jiaying Liu, Zongming Guo, and Shuicheng Yan. 2017. Deep joint rain detection and removal from a single image. In *CVPR*. 1357–1366.
- [55] Yong Yang, Juwei Guan, Shuying Huang, Weiguo Wan, Yating Xu, and Jiaying Liu. 2021. End-to-End Rain Removal Network Based on Progressive Residual Detail Supplement. *IEEE Trans. Multimedia* (2021).
- [56] Rajeev Yasarla and Vishal M Patel. 2019. Uncertainty guided multi-scale residual learning—using a cycle spinning cnn for single image de-raining. In *Proceedings of the IEEE/CVF Conference on Computer Vision and Pattern Recognition*. 8405–8414.
- [57] Weijiang Yu, Zhe Huang, Wayne Zhang, Litong Feng, and Nong Xiao. 2019. Gradual network for single image de-raining. In *ACM Multimedia*. 1795–1804.
- [58] Yi Yu, Wenhao Yang, Yap-Peng Tan, and Alex C Kot. 2022. Towards Robust Rain Removal Against Adversarial Attacks: A Comprehensive Benchmark Analysis and Beyond. *arXiv preprint arXiv:2203.16931* (2022).
- [59] Syed Waqas Zamir, Aditya Arora, Salman Khan, Munawar Hayat, Fahad Shahbaz Khan, and Ming-Hsuan Yang. 2021. Restormer: Efficient Transformer for High-Resolution Image Restoration. *arXiv preprint arXiv:2111.09881* (2021).
- [60] Syed Waqas Zamir, Aditya Arora, Salman Khan, Munawar Hayat, Fahad Shahbaz Khan, Ming-Hsuan Yang, and Ling Shao. 2021. Multi-Stage Progressive Image Restoration. In *CVPR*. 14821–14831.
- [61] Han Zhang, Ian Goodfellow, Dimitris Metaxas, and Augustus Odena. 2019. Self-attention generative adversarial networks. In *International conference on machine learning*. PMLR, 7354–7363.
- [62] He Zhang and Vishal M Patel. 2017. Convolutional sparse and low-rank coding-based rain streak removal. In *WACV*. 1259–1267.
- [63] He Zhang and Vishal M Patel. 2018. Density-aware single image de-raining using a multi-stream dense network. In *CVPR*. 695–704.
- [64] He Zhang, Vishwanath Sindagi, and Vishal M Patel. 2020. Image de-raining using a conditional generative adversarial network. *IEEE Trans. Circuits Syst. Video Technol.* 30, 11 (2020), 3943–3956.
- [65] Yulun Zhang, Yapeng Tian, Yu Kong, Bineng Zhong, and Yun Fu. 2018. Residual dense network for image super-resolution. In *CVPR*. 2472–2481.
- [66] Xian Zhong, Shidong Tu, Xianzheng Ma, Kui Jiang, Wenxin Huang, and Zheng Wang. 2022. Rainy WCity: A Real Rainfall Dataset with Diverse Conditions for Semantic Driving Scene Understanding. In *Proc. IJCAI Int. Joint Conf. Artif. Intell.*
- [67] Xian Zhong, Shilei Zhao, Xiao Wang, Kui Jiang, Wenxuan Liu, Wenxin Huang, and Zheng Wang. 2021. Unsupervised Vehicle Search in the Wild: A New Benchmark. In *Proceedings of the 29th ACM International Conference on Multimedia*. 5316–5325.